

TIN2 deficiency leads to ALT-associated phenotypes and differentiation defects in embryonic stem cells

Shanshan Yin,^{1,2} Fangyingnan Zhang,¹ Song Lin,¹ Wei Chen,¹ Kai Weng,³ Dan Liu,⁴ Chuanle Wang,¹ Zibin He,¹ Yuxi Chen,¹ Wenbin Ma,¹ Junjiu Huang,¹ Yan Huang,^{1,*} and Zhou Songyang^{1,2,5,*}

¹MOE Key Laboratory of Gene Function and Regulation, Guangzhou Key Laboratory of Healthy Aging Research, SYSU-BCM Joint Research Center, School of Life Sciences, Sun Yat-sen University, Guangzhou 510275, China

²Sun Yat-sen Memorial Hospital, Sun Yat-sen University, Guangzhou 510120, China

³Shanghai Institute of Precision Medicine, Shanghai 200125, China

⁴Verna and Marrs Mclean Department of Biochemistry and Molecular Biology, Baylor College of Medicine, One Baylor Plaza, Houston, TX 77030, USA

⁵Bioland Laboratory (Guangzhou Regenerative Medicine and Health Guangdong Laboratory), Guangzhou 510005, China

*Correspondence: huangy336@mail.sysu.edu.cn (Y.H.), songyanz@mail.sysu.edu.cn (Z.S.)

<https://doi.org/10.1016/j.stemcr.2022.03.005>

SUMMARY

Telomere integrity is critical for embryonic development, and core telomere-binding proteins, such as TIN2, are key to maintaining telomere stability. Here, we report that homozygous *Tin2*^{S341X} resulted in embryonic lethality in mice and reduced expression of *Tin2* in the derived mouse embryonic stem cells (mESCs). Homozygous mutant mESCs were able to self-renew and remain undifferentiated but displayed many phenotypes associated with alternative lengthening of telomeres (ALT), including excessively long and heterogeneous telomeres, increased ALT-associated promyelocytic leukemia (PML) bodies, and unstable chromosomal ends. These cells also showed upregulation of *Zscan4* expression and elevated targeting of DAXX/ATRAX and H3K9me3 marks on telomeres. Furthermore, the mutant mESCs were impeded in their differentiation capacity. Upon differentiation, DAXX/ATRAX and PML bodies disassociated from telomeres in these cells, where elevated DNA damage was also apparent. Our results reveal differential responses to telomere dysfunction in mESCs versus differentiated cells and highlight the critical role of TIN2 in embryonic development.

INTRODUCTION

Mammalian telomere DNA consists of tandem TTAGGG repeats and is regulated and protected by myriad factors, including telomerase and the six-protein complex composed of TRF1, TRF2, TIN2/TIN2, POT1, TPP1, and RAP1 (de Lange, 2005; Liu et al., 2004). To achieve unlimited growth, most tumor cells reactivate telomerase to maintain their telomere length. However, about 10%–15% of human cancers use the telomerase-independent alternative lengthening of telomere (ALT) mechanism (Shay and Wright, 2019). During the two-cell stage in mouse embryonic development, embryos are telomerase inactive and use the ALT mechanism to elongate telomeres (Falco et al., 2007; Zalzman et al., 2010). Mouse embryonic fibroblasts (MEFs) and embryonic stem cells (ESCs) derived from *Terc*^{-/-} mice have also been reported to activate the ALT mechanism (Niida et al., 2000). These findings support an important role for ALT in mouse embryonic development.

Pathogenic mutations in telomerase subunits and telomere-binding proteins have been found to disrupt telomere maintenance and contribute to numerous human diseases, such as dyskeratosis congenita (DC) and cancer (Martinez and Blasco, 2017). In human cells, TIN2 bridges different telomere-binding activities for telomere length regulation and end protection. For example, it can stabilize

TRF1/TRF2 and TPP1/POT1 complexes on telomeres (Kim et al., 1999, 2004) and negatively regulate telomere length by modulating telomerase recruitment (Frank et al., 2015; Ye and de Lange, 2004). Many *TIN2* pathogenetic mutations were identified in patients with DC, pulmonary fibrosis, or rarer cases of cancer (He et al., 2020; Savage et al., 2008; Schmutz et al., 2020; Walne et al., 2008).

Telomere integrity is vital for embryonic development. Individual abrogation of *Trf1* (Karlseder et al., 2003), *Trf2* (Celli and de Lange, 2005), *Tpp1* (Kibe et al., 2010), or *Pot1a* (Hockemeyer et al., 2006) led to embryonic lethality. In the case of *Tin2*, complete loss resulted in embryonic lethality at embryonic day 3.5 (E3.5)–E7.5 (Chiang et al., 2004). Furthermore, the derivation of mouse ESC (mESC) lines from *Tin2*^{-/-} blastocytes was unsuccessful due to severe growth defects during the early stages of mESC establishment (Chiang et al., 2004). The deletion of *Tin2* in human cells and mouse fibroblast cells could cause severe DNA damage and cell growth defects (Celli and de Lange, 2005; Kim et al., 2008, 2017). Interestingly, recent studies showed that *Trf2* knockout (KO) in mESCs did not result in cell death or end-to-end chromosome fusions (Markiewicz-Potoczny et al., 2020; Ruis et al., 2020), suggesting that ESCs and somatic cells may respond to telomere dysfunction differently and that further work is needed to investigate such differences.





The predominant human TIN2 short isoform TIN2S is more widely studied and encoded by the first six exons of the *TINF2/TIN2* gene, whereas the longer TIN2L isoform utilizes all nine exons (Kaminker et al., 2009). The mouse *Tinf2/Tin2* locus is similarly organized as its human counterpart, where all nine exons are present without producing any apparent shorter isoforms (Nelson et al., 2018). When we introduced a premature termination mutation (*Tin2*^{S341X}) into the *Tinf2/Tin2* locus in mice to study the contribution of *Tin2* exon 7–9, we found that homozygous *Tin2*^{S341X} mutation resulted in embryonic lethality. The derived mESC lines showed drastically reduced *Tin2* expression but were nonetheless able to self-renew and maintain their undifferentiated state. These mutant mESCs displayed many ALT-associated characteristics and increased DAXX/ATR recruitment and H3K9me3 occupancy on telomeres. Moreover, the ability of the mutant mESCs to differentiate *in vitro* and *in vivo* was impaired. In mutant cells, differentiation induction led to the reduced association of DAXX/ATR and promyelocytic leukemia (PML) bodies with telomeres and widespread DNA damage. Finally, both TIN2L and TIN2S could bind to telomeres efficiently, and re-introducing either isoform rescued the *Tin2*^{S341X} mESCs in the assays we performed. These findings illustrate the important role of TIN2 in the regulation of telomeres and differentiation in mESCs and suggest comparable functions of TIN2S and TIN2L in mESC telomere maintenance.

RESULTS

Tin2^{S341X} mutation reduces *Tin2* expression and leads to embryonic lethality in mice

We used the CRISPR-Cas9 technology to introduce a stop codon at the 5' end of exon 7 in the mouse *Tin2* locus (Figure S1A) and herein refer to wild-type mice as *Tin2*^{WT}, heterozygous mice as *Tin2*^{WT/S341X}, and homozygous mutants as *Tin2*^{S341X}. Of the 315 pups obtained from crossing *Tin2*^{WT/S341X} mice, no *Tin2*^{S341X} animals were obtained, whereas the ratio of wild-type to heterozygous progeny was roughly 1:2 (Figure 1A). Heterozygous mice developed normally with no notable differences from *Tin2*^{WT} mice. We then genotyped the embryos from heterozygous intercrosses at selected time points (Figure 1B). Among E3.5 embryos, the observed ratio of the three expected genotypes was consistent with Mendel's law of segregation. By E10.5, however, no homozygous mutant embryos could be found. Only a single dead homozygous mutant embryo was found at E7.5, suggesting that death of *Tin2*^{S341X} embryos likely occurred between E3.5 and E7.5.

To probe the impact of the *Tin2*^{S341X} mutation in early development, we established mESC lines of all three

genotypes from blastocysts by crossing *Tin2*^{WT/S341X} mice, including two homozygous *Tin2*^{S341X} lines obtained in two independent experiments (Figure S1B). Both wild-type and mutant mESC lines appeared normal in morphology and grew as colonies. Since heterozygous mice developed normally, we focused on the homozygotes and the two matched *Tin2*^{WT} control lines hereafter.

When we analyzed the mESCs by qRT-PCR using primers spanning exons 1–2 (primer 1) or 5–6 (primer 2), we observed decreased *Tin2* transcripts in mutant cells (Figure 1C), which was corroborated by significantly reduced protein levels in immunofluorescence (IF)-fluorescence *in situ* hybridization (FISH) assays using an antibody that has been shown to recognize mouse TIN2 proteins in immunostaining assays (Figures 1D and 1E). Taken together with reduced *Tin2* mRNA levels, this downregulation of TIN2 protein expression in *Tin2*^{S341X} mESCs is likely due to cellular protective mechanisms, such as nonsense-mediated mRNA decay, and points to TIN2 deficiency in the mutant mESCs (Lykke-Andersen and Jensen, 2015). Given the importance of TIN2 in stabilizing core telomeric complexes, we also examined the telomeric targeting of TRF1 and TRF2 but found no difference between mutant and wild-type mESCs (Figures S1C and S1D), suggesting that TRF1/TRF2 binding to telomere DNA remained largely unchanged despite decreased *Tin2* expression in *Tin2*^{S341X} cells. Then, we ectopically expressed SFB-tagged mouse TIN2 proteins that correspond to either TIN2L or TIN2S in *Tin2*^{S341X} mutant mESCs (Figure S1E) and examined their telomere binding efficiencies by telomere chromatin immunoprecipitation (ChIP) using an anti-FLAG antibody. We found similar telomere signal intensities were detected in TIN2L- and TIN2S-overexpressing cells, suggesting that lacking exons 7–9 did not affect TIN2 telomere binding (Figures 1F and 1G).

Tin2^{S341X} mESCs harbor longer telomeres and display ALT-associated characteristics

To understand how the *Tin2*^{S341X} mutation might affect TIN2 function, we carried out telomere restriction fragment (TRF) analysis by pulsed-field gel electrophoresis (PFGE) in various mESC lines. Compared with wild-type as well as heterozygous mESCs, the median telomere length in the two homozygous mutant mESC lines was considerably longer (Figure 2A). The quantitative FISH (Q-FISH) assay again found *Tin2*^{S341X} mESCs to harbor significantly longer and more heterogeneously distributed telomeres than wild-type cells (Figures 2B and 2C). These results combined indicate abnormal telomere lengthening in *Tin2*^{S341X} mESCs. To determine whether it was the result of abnormal telomerase activities, we carried out telomeric repeat amplification protocol (TRAP) assays, but *Tin2*^{S341X}

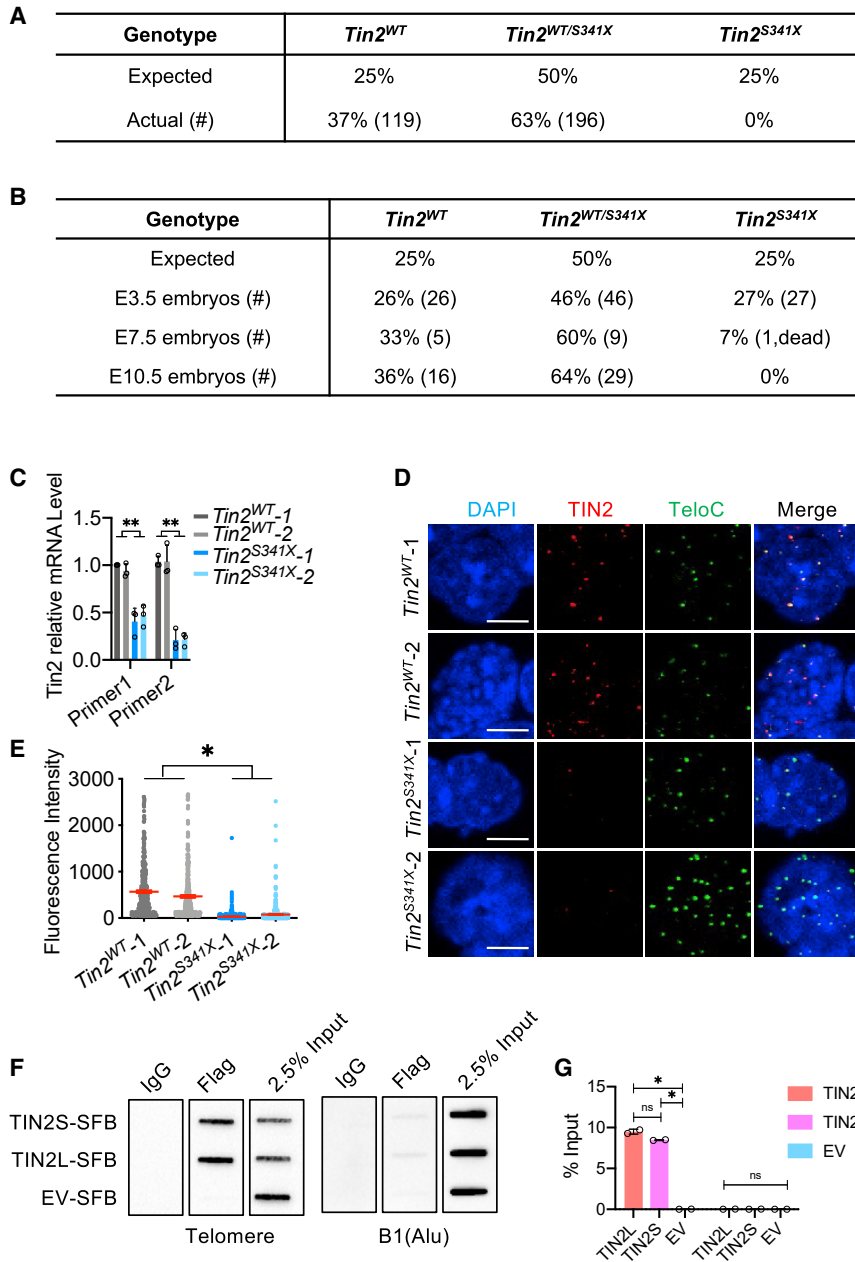


Figure 1. Homozygous *Tin2*^{S341X} mutation is embryonically lethal in mice

(A) The number and percentage of offspring with the expected versus actual genotypes from *Tin2*^{WT/S341X} breeding pairs are listed.

(B) The number and percentage of early embryos at different stages from *Tin2*^{WT/S341X} intercrosses are listed.

(C) *Tin2* mRNA expression in various mESC lines was analyzed by qPCR. Three independent experiments were performed. Error bars indicate SD.

(D) mESCs were analyzed by IF-FISH using an antibody that can recognize mouse TIN2 in IF assays (red) and a telomere probe (green). Scale bars: 5 μ m.

(E) Fluorescence intensities of TIN2 signals in samples from (D) were measured and plotted, with each dot representing one TIN2 focus. Red line indicates mean intensity of each sample. Around 20 cells for each line were examined.

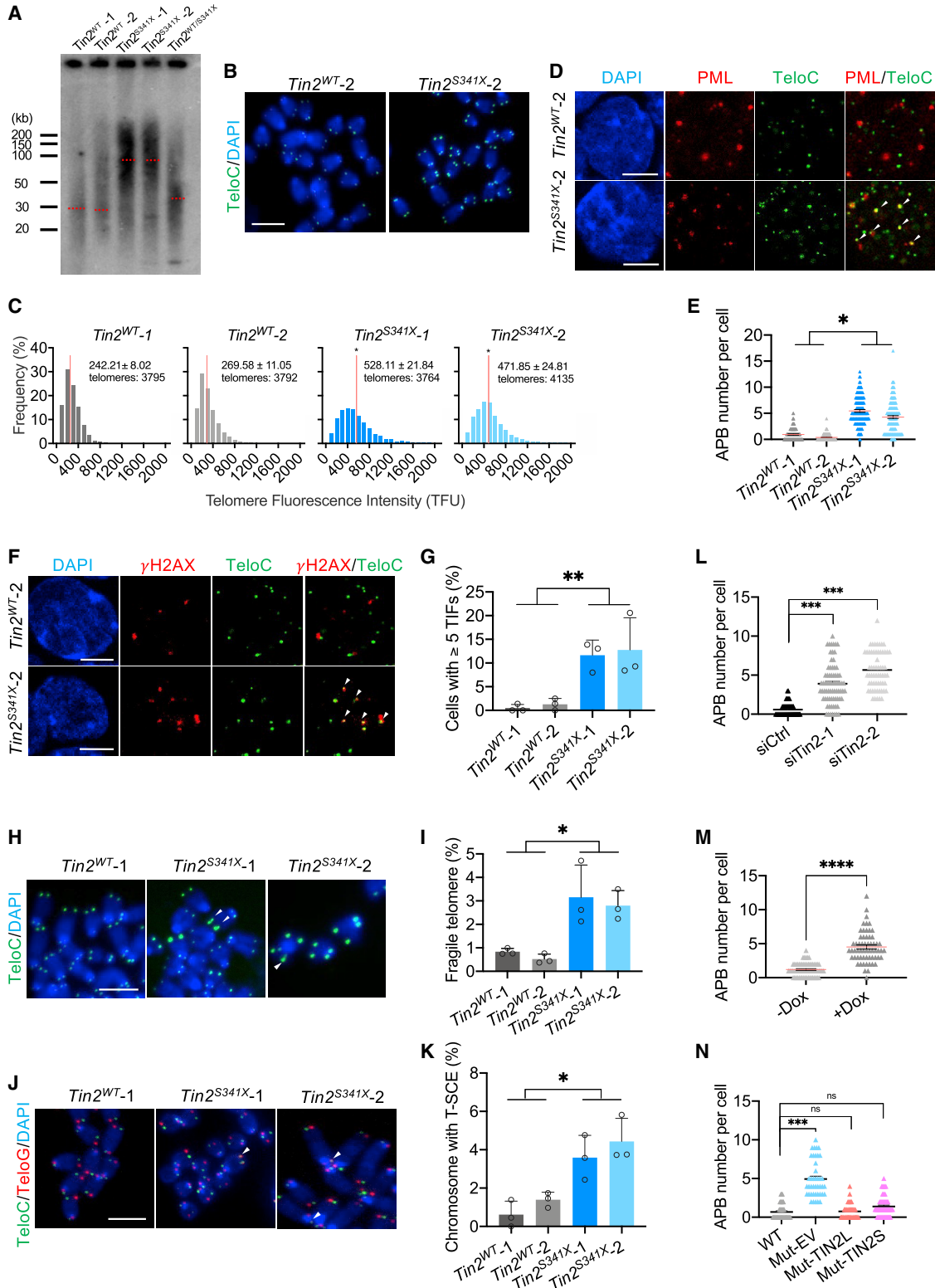
(F) *Tin2*^{S341X} mESCs ectopically expressing SFB-tagged TIN2S, TIN2L, or empty vector control (EV) were analyzed in telomere ChIP assays using an anti-FLAG antibody. Coprecipitated DNA was slot blotted and then hybridized with telomere or B1(Alu) probes. Representative images are shown. EV-SFB served as negative control.

(G) Data from (F) were quantified and plotted and represent results from two technical replicates. Error bars indicate SD.

For (C and E), statistical significance was determined by t test. For (G), one-way ANOVA was used. For all panels, * $p < 0.05$ and ** $p < 0.01$. Not significant (ns), $p > 0.05$.

mESCs appeared similar to control cells (Figure S2A). We noticed mutant mESCs exhibited a drastic increase in telomere-associated PML bodies (APBs) (Figures 2D, 2E, and S2B). Increased APBs and extremely long and heterogeneous telomeres are two hallmarks of ALT cancer cells (Bryan et al., 1995; Yeager et al., 1999), which often contain increased telomere dysfunction-induced foci (TIF), fragile telomeres due to DNA replication stress, and higher frequencies of telomere sister chromatid exchange (T-SCE) and formation of extrachromosomal circular telomeric DNA called C-circle (Cesare and Griffith, 2004; Henson

et al., 2009; Londono-Vallejo et al., 2004; Takai et al., 2003). To assess whether such phenotypes could also be observed in *Tin2*^{S341X} mESCs, we first co-stained the cells for γ -H2AX and telomeres. Significantly more *Tin2*^{S341X} mESCs appeared to harbor ≥ 5 TIFs than control cells (Figures 2F and 2G). In FISH assays, both *Tin2*^{S341X} mESC lines exhibited more fragile telomeres than wild-type cells as well (Figures 2H and 2I). Consistent with their heterogeneous telomere length distribution, *Tin2*^{S341X} mESCs also exhibited more frequent T-SCE events, as evidenced by increased overlapping signals in cells co-stained with



(legend on next page)



telomere C- and G-strand probes (Figures 2J and 2K). C-circle formation assays via ϕ 29 amplification and slot blotting, however, revealed no significant differences between *Tin2*^{WT} and *Tin2*^{S341X} cells (Figures S2C and S2D). It has been reported that some telomerase-positive tumors with APBs contain no C-circles and that forced expression of hTERT in ALT tumors can reduce C-circles to non-ALT levels (Plantinga et al., 2013). Our results collectively showed that, despite the presence of active telomerase in the mutant mESCs, the *Tin2*^{S341X} mutation led to many ALT-associated characteristics.

To further determine how TIN2 deficiency might be responsible for the ALT-associated phenotypes, we first knocked down *Tin2* in wild-type mESCs and examined the level of APBs in these cells. With efficient inhibition, TIN2 foci became undetectable in IF-FISH assays, which was concurrent with an increase in the number of APBs (Figures 2L, S2E, and S2F). Next, we generated inducible *Tin2* CRISPR KO mESCs. Following doxycycline (Dox) addition, which activated Cas9-mediated *Tin2* KO, TIN2 foci again became undetectable in IF-FISH assays, which coincided with the increase in APBs (Figures 2M and S2G). The level of APBs in *Tin2* knockdown (KD) and KO cells was similar to that in *Tin2*^{S341X} cells. Interestingly, in *Tin2*^{S341X} mutant mESCs, re-introducing mouse TIN2 proteins that correspond to either TIN2L or TIN2S effectively reduced the number of APBs to levels in *Tin2*^{WT} cells (Figures S1E and 2N versus 2E), indicating that TIN2 deficiency was responsible for the ALT-associated phenotypes in mutant cells and that the two TIN2 isoforms may have comparable roles.

Increased telomeric H3K9me3 marks and DAXX/ATRAX recruitment in *Tin2*^{S341X} mESCs

Global DNA demethylation has been linked to increased ALT-associated telomere elongation and recombination in mESCs (Gonzalo et al., 2006), but when we measured cytosine DNA methylation levels at subtelomeric regions on Chr1 and Chr16 (Gonzalo et al., 2006), we saw no difference between wild-type and mutant mESCs (Figure S3A). Although we cannot exclude the possibility that differential DNA methylation levels may be present in other subtelomeric regions, these results point to minimal effects on subtelomeric DNA methylation with the *Tin2*^{S341X} mutation.

In mESCs, it has been reported that increased telomeric H3K9me3 may promote the appearance of ALT features (Gauchier et al., 2019). In *Tin2*^{S341X} mESCs, H3K9me3 ChIP brought down more telomere DNA signals compared with control cells but showed no difference when B1 repeat sequences (human Alu homologues) were examined (Figures 3A and 3B). In comparison, signal intensities for telomeres and B1 repeats were similar between mutant and control mESCs in H3 ChIP samples (Figures 3A and 3B). The establishment of H3K9me3 marks on telomeres depends on histone methyltransferases as well as DAXX/ATRAX complex that can localize to heterochromatin (Lewis et al., 2010). We showed previously that, in *Dnmt1/Dnmt3a/Dnmt3b* triple-KO mESCs, the DAXX/ATRAX complex became enriched at telomeres and in turn recruited histone methyltransferases and upregulated H3K9me3 marks on telomeres (He et al., 2015). IF-FISH analysis of the mutant mESCs revealed more co-localization of DAXX and ATRAX with

Figure 2. Mutant mESCs display ALT-associated phenotypes

- (A) Telomere length was detected using PFGE-TRF in mESCs at passage 26 (P26). Red dash lines indicate median telomere length.
- (B) The telomere length was measured by Q-FISH. Telomere DNA was hybridized to an FITC-labeled telomere probe (green), and chromosomes were stained by DAPI (blue). Representative images from each genotype are shown.
- (C) Quantification of telomere fluorescence units (TFUs) of experiments from (B). Mean TFU \pm SD and total number of telomeres from three technical replicates are listed. Red line indicates mean TFU.
- (D) mESC lines were examined by IF-FISH using an anti-PML antibody (red) and a telomere probe (green). Representative images from each genotype are shown. White arrowheads indicate foci with overlapping signals.
- (E) Quantification of telomere-associated PML bodies (APBs) from (D). The number of APBs per cell is shown with mean \pm SEM.
- (F) Various mESC lines were examined by IF-FISH with an anti- γ H2AX antibody (red) and a telomere probe (green). Representative images from each genotype are shown. White arrowheads indicate foci with overlapping signals.
- (G) The percentage of cells with ≥ 5 TIFs was quantified and plotted. Error bars indicate SD.
- (H) Various mESC lines were stained with a telomere probe (green) to detect fragile telomeres (doublet or smear). Representative images are shown. Arrowheads indicate fragile telomeres.
- (I) Quantification of data from (H) (>820 chromosomes). Error bars indicate SD.
- (J) Various mESC lines were examined by chromosome orientation FISH (CO-FISH) to detect T-SCE with telomere C-strand (green) and G-strand (red) probes. Representative images are shown here. Arrowheads indicate T-SCEs.
- (K) Quantification of data from (J) (>620 chromosomes). Error bars indicate SD.
- (L and M) APBs were examined and quantified in *Tin2*^{WT} mESC treated with siTin2 (L) or with or without (+/–) Dox (M).
- (N) APBs were examined and quantified in *Tin2*^{WT} and *Tin2*^{S341X} ectopically expressing TIN2L, TIN2S, or empty vector (EV).
- For (L and N), one-way ANOVA was used for statistical analysis. For all other panels, t test was used. Data were from three independent experiments. * $p < 0.05$; ** $p < 0.01$; *** $p < 0.001$; **** $p < 0.0001$; ns, $p > 0.05$. All scale bars are 5 μ m.

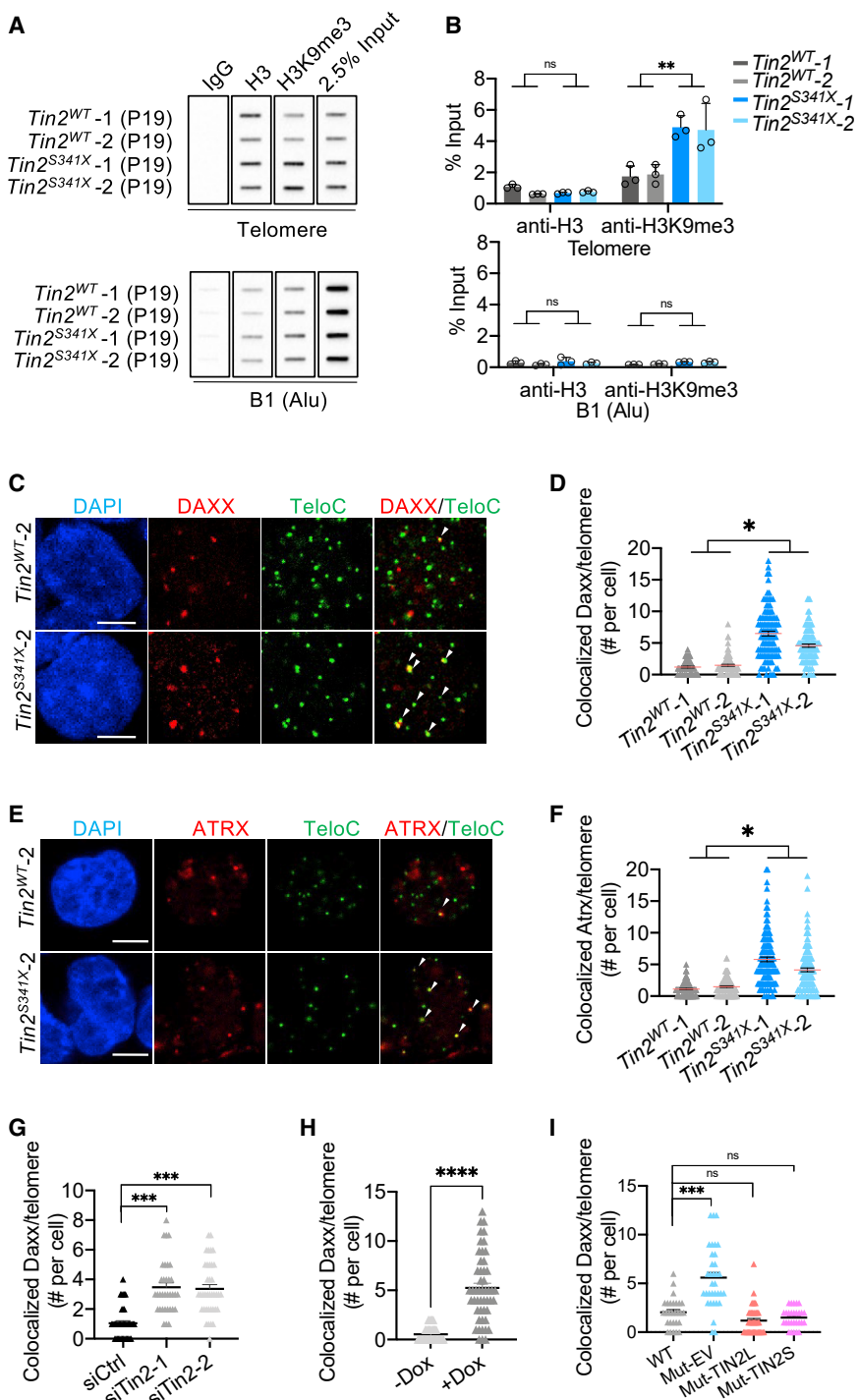


Figure 3. Telomeric occupancy of H3K9me3 and DAXX/ATR increases in mutant mESCs

(A) Control and mutant mESCs were analyzed in telomere ChIP assays using antibodies against H3K9me3 and H3. Coprecipitated DNA was slot blotted and then hybridized with telomere or B1 probes. H3 served as an internal control. IgG served as a negative control.

(B) Data from (A) were quantified. Error bars indicate SD.

(C–F) The localization of DAXX (C) and ATRX (E) was determined by IF-FISH with an anti-DAXX/ATR antibody (red) and a telomere probe (green). Representative images from each genotype are shown with scale bars of 5 μ m. Arrowheads indicate co-localized foci. Co-localization of DAXX (D) and ATRX (F) with telomeres in each cell was quantified and plotted. Lines are mean \pm SEM.

(G and H) Localization of DAXX was examined and quantified in *Tin2*^{WT} mESCs treated with siRNAs (G) or with or without (+/–) Dox (H).

(I) Localization of DAXX was examined and quantified in *Tin2*^{WT} and *Tin2*^{S341X} ectopically expressing TIN2L, TIN2S, or empty vector (EV).

For (G and I), one-way ANOVA was used for statistical analysis. For all other panels, t test was used. Data were from three independent experiments. * $p < 0.05$; ** $p < 0.01$; *** $p < 0.001$; **** $p < 0.0001$; ns, $p > 0.05$.

telomere signals compared with wild-type cells (Figures 3C–3F). Higher telomere signal intensities were also detected in DAXX ChIP in mutant mESCs (Figures S3B and S3C). IF-FISH showed that telomeric DAXX foci increased to levels seen in *Tin2*^{S341X} mESCs when *Tin2*^{WT} mESCs were treated with small interfering RNAs (siRNAs) targeting *Tin2* or

when *Tin2* was inducibly knocked out (Figures 3G and 3H versus 3D). Ectopically expressing TIN2L or TIN2S in mutant mESCs reduced telomeric DAXX signals as in *Tin2*^{WT} cells (Figure 3I), supporting the idea that TIN2 reduction caused by *Tin2*^{S341X} mutation led to the enrichment of DAXX on telomeres.

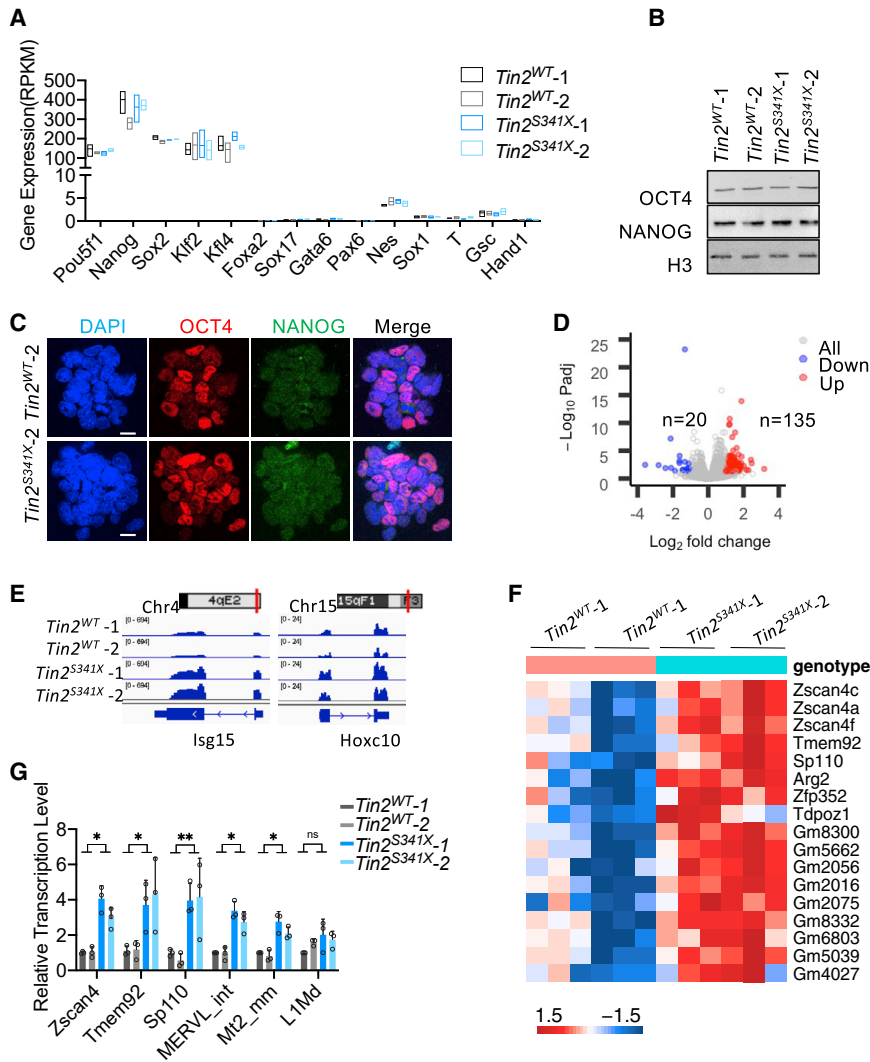


Figure 4. Transcriptomic analysis of *Tin2^{S341X}* mESC lines

RNA-seq was carried out in four mESC lines with three technical replicates for each genotype.

(A) Reads per kilobase of transcript per million mapped reads (RPKM) values for a select list of genes are shown in bar graphs. The middle line indicates mean RPKM. No statistical difference was detected.

(B and C) mESCs were examined by immunoblotting (B) and immunostaining (C) using antibodies against OCT4 and NANOG. H3 blotting was used as the loading control. Scale bars: 20 μ m.

(D) The statistical significance of gene expression changes in mutant mESCs was graphed in a volcano plot where each dot represents a single gene. Red and blue indicate significantly up- and down-regulated genes, respectively.

(E) The coverage of *Isg15* and *Hoxc10* was visualized using the Integrative Genomics Viewer. Red lines indicate chromosomal locations of the genes.

(F) Heatmap showing the expression (\log_2 RPKM) of 2C-associated genes in mESCs.

(G) The expression of several 2C-associated genes and transposable elements (TEs) was measured by qPCR analysis from three independent experiments.

Error bars indicate SD; t test was used for statistical analysis. * $p < 0.05$; ** $p < 0.01$; *** $p < 0.001$; ns, $p > 0.05$.

Tin2^{S341X} mESCs upregulate the expression of subtelomeric and 2C-related genes

To better understand the changes that occurred in *Tin2^{S341X}* mESCs, we carried out RNA sequencing (RNA-seq) to analyze their transcriptome. In both mutant and wild-type mESCs, pluripotency markers were similarly highly expressed, whereas markers for differentiated germ layers were expressed at low levels (Figure 4A). Indeed, the *Tin2^{S341X}* lines expressed OCT4 and NANOG at levels similar to controls (Figures 4B, 4C, S4A, and S4B) when analyzed by indirect immunoblotting and immunofluorescence and exhibited alkaline phosphatase activities as well (Figures S4C and S4D). These results indicate that *Tin2^{S341X}* mESCs were able to maintain the undifferentiated state.

RNA-seq analysis also revealed an overall increase in gene expression in the mutant cells, where 87% (135/155) of the differentially expressed genes were upregulated

($p_{\text{adj.}} < 0.05$; $\log_2(\text{fold change}) > 1$; Figure 4D). Gene ontology analysis showed those genes are enriched in processes of cellular responses to heat and translation initiation (Figure S4E). Of the genes with elevated expression, 17 (12.6%) are located in subtelomeric regions (<10 Mb from chromosomal ends; Figure S4F), including *Isg15* and *Hoxc10*, two genes respectively located in the subtelomeric regions of chr4 and chr15 (Figure 4E). In upregulated genes, the odds ratio of subtelomeric genes compared with non-subtelomeric genes is 1.696 ($p = 0.042$), indicating higher sensitivity of genes in subtelomeric regions to the *Tin2* mutation (Figure S4G).

Notably, *Zscan4* family members, including *Zscan4a*, *Zscan4c*, and *Zscan4f*, were upregulated in mutant mESCs (Figure 4F). High-level expression of *Zscan4* is a characteristic of two-cell (2C)-stage embryos, which utilize the ALT mechanism for telomere elongation (Falco et al., 2007).



Indeed, several 2C-embryo-specific genes were upregulated in mutant mESCs as well (Figure 4F; Hung et al., 2013; Macfarlan et al., 2012). The heightened expression of *Zscan4*, *Tmem92*, and *Sp110* was also validated by the qPCR assay (Figure 4G). In mESCs, telomerase deficiency or global DNA damage can induce *Zscan4* expression (Huang et al., 2011; Storm et al., 2014). In turn, ZSCAN4 can facilitate telomere recombination to prevent excessive telomere shortening (Zalzman et al., 2010). ZSCAN4 can also bind to mouse endogenous retrovirus *MERVL/Mt2* in mESCs and activate its expression (Zhang et al., 2019). The activation of endogenous retrovirus thus is another hallmark of 2C embryos and 2C-state mESCs (Macfarlan et al., 2012). qPCR analysis showed that *MERVL_int* and *Mt2_mm* were indeed upregulated in mutant mESCs, whereas the expression of *L1Md* repeats, which are not specific to the 2C stage, remained similar among different mESC lines (Figure 4G). Ectopically expressing TIN2L or TIN2S in mutant mESCs downregulated *Zscan4*, *Tmem92*, *MERVL-int*, and *Mt2_mm* expression (Figure S4H), while *Tin2* inducible KO mESCs showed a moderate increase of several 2C genes after 48 h of Dox treatment (Figure S4I). These data suggest that the transcriptional changes caused by the *Tin2*^{S341X} mutation are more likely a result of reduced TIN2 expression.

Tin2^{S341X} mESCs exhibit impaired differentiation capacity

We noticed early in our study that *Tin2*^{S341X} cells grew more slowly and had lower rates of EdU uptake than control cells (Figures S5A and S5B). We have shown previously that TIN2 can localize to mitochondria and regulate ATP metabolism in human cells and that TIN2 inhibition can negatively affect cell growth (Chen et al., 2012; Kim et al., 2017). Therefore, we examined ATP and reactive oxygen species (ROS) production in our mESC lines (Figures S5C and S5D). No obvious difference between wild-type and mutant cells was detected, suggesting that ATP metabolism likely remained unaffected and did not contribute to the slower growth of the mutant cells.

Despite the modest growth difference, mutant mESCs were able to proliferate for extended passages while maintaining their undifferentiated state (Figures 4A–4C). We then carried out teratoma assays in nude mice to investigate the differentiation capacity of the mESC lines. As shown in Figure 5A, teratomas were observed in five out of six nude mice in the wild-type group but none in the mutant group, suggesting that the *Tin2*^{S341X} mutation impeded the differentiation capacity of mESCs. Next, we investigated these cells using the embryoid body (EB) formation assay. Both wild-type and mutant ESCs were able to form EBs with no apparent cell death during 8 days of culturing in low-attachment dishes (Figure S5E).

As expected, pluripotency markers, such as *Pou5f1* and *Nanog*, decreased in wild-type cells as they became more differentiated, accompanied by increased expression of various germ layer markers (Figure 5B). In comparison, although *Tin2*^{S341X} mutant cells also downregulated pluripotency markers as days progressed, the expression level of germ layer markers was significantly lower (Figure 5B), indicating a block in differentiation pathways. In mutant mESCs, overexpressing TIN2L and TIN2S, but not empty vector, increased germ layer marker expression significantly after EB differentiation (Figure 5C), indicating that the differentiation defects in mutant mESCs loss could be rescued by either TIN2 isoform.

Tin2^{S341X} embryos died shortly after reaching the E3.5 blastocyst stage (Figure 1B). In mouse embryos, the neural plate forms around E5.5–E7.5 (Hitoshi et al., 2004). When we differentiated the mESCs into ectoderm lineage, both wild-type and mutant cells downregulated the expression of pluripotency markers *Nanog* and *Pou5f1* (Figure S5F). Compared with control cells, however, the expression of neural progenitor markers *Nes* and *Pax6* was significantly lower in mutant cells (Figure S5F), supporting the notion that *Tin2*^{S341X} cells were impaired in differentiation capacity.

Tin2^{S341X} mutation leads to widespread DNA damage upon differentiation

In undifferentiated *Tin2*^{S341X} mESCs, we observed increased telomeric targeting of PML bodies and DAXX/ATRAX proteins (Figures 2D, 2E, and 3C–3F). By day 12 following ectoderm differentiation induction, co-staining signals of DAXX/ATRAX proteins and PML bodies with telomeres in mutant cells had dropped to levels similar to control cells (Figures 6A–6D, S6A, and S6B). PML bodies are known to play critical roles in DNA damage response and chromatin stability modulation on both telomeres and other genomic regions (Dellaire et al., 2006; Marchesini et al., 2016). Likewise, DAXX and ATRAX can coordinate with other proteins to maintain genome stability in tumor cells and mESCs (He et al., 2015; Juhasz et al., 2018). We reasoned that following differentiation, with the disassociation of DAXX/ATRAX proteins and PML bodies from telomeres, telomere chromatin might become more susceptible to damage. Indeed, Q-FISH revealed more fragile telomeres and chromosome fusions in differentiated cells derived from mutant mESCs (Figures S6C and S6D). When differentiated cells were co-stained for γ H2AX and telomeres, overlapping γ H2AX and telomere signals remained higher in mutant cells (Figures 6E and 6F), at levels similar to those observed in undifferentiated *Tin2*^{S341X} mESCs (Figures 2F and 2G). Notably, a considerable proportion of the differentiated *Tin2*^{S341X} cells also exhibited high levels of pan-nuclear staining of γ H2AX (Figures 6G and 6H), an indication

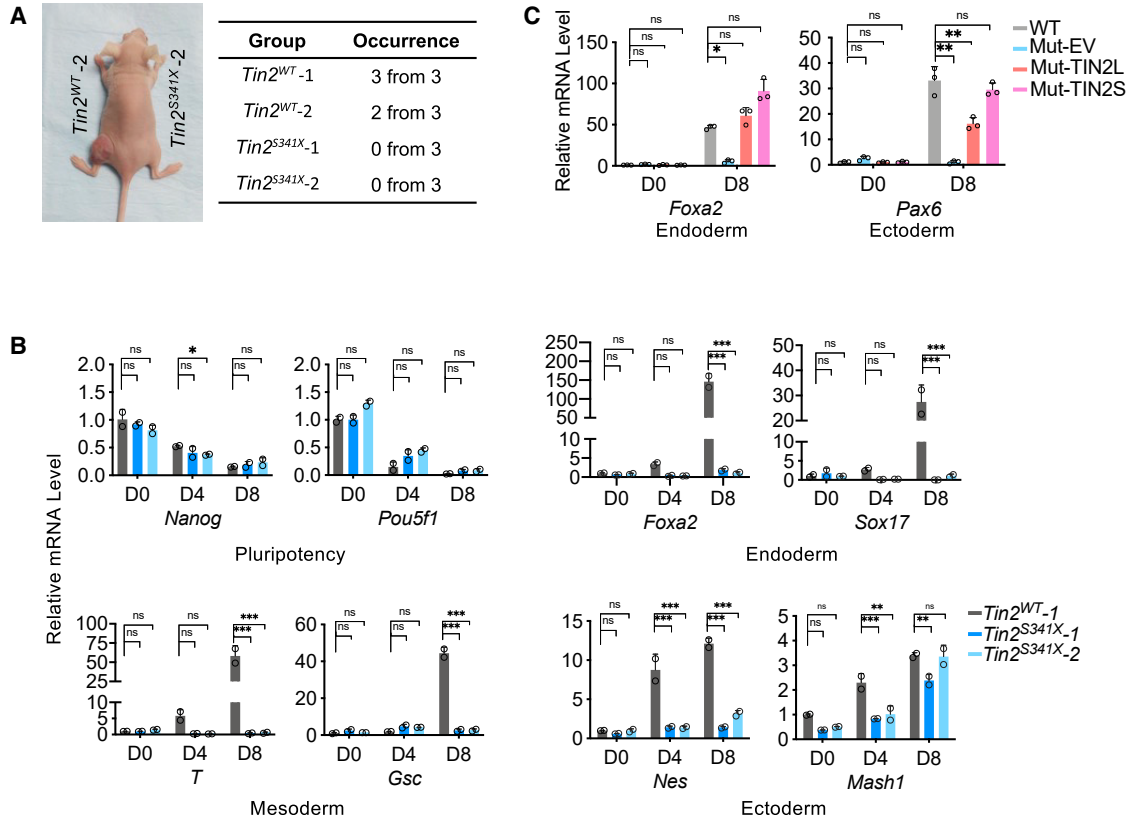


Figure 5. Mutant mESCs show impaired differentiation capacity

(A) mESCs were injected into the hind legs of nude mice to evaluate their capacity to form teratomas, with wild-type mESCs on the left and mutant mESCs on the right.

(B) During EB formation assays, cells were collected at the indicated time points for qPCR analysis of various marker genes. Two technical replicates are shown.

(C) qPCR was used to detect germ layer marker expression in *Tin2*^{WT} and *Tin2*^{S341X} ectopically expressing TIN2L, TIN2S, or empty vector (EV). For all panels, two-way ANOVA was used for statistical calculation. **p* < 0.05; ***p* < 0.01; ****p* < 0.001; ns, *p* > 0.05. Error bars indicate SD.

of severe DNA damage, replication stress, and/or pre-apoptosis (de Feraudy et al., 2010; Moeglin et al., 2019). Such pan-nuclear γ H2AX signals were absent in undifferentiated mESCs, where only clustered γ H2AX foci were visible (Figure 2F). These findings suggest possible links between genome-wide instability and increased telomeric disassociation of DAXX/ATR proteins and PML bodies and led us to examine ESCs depleted of *Daxx* or *Pml*. Efficient KD of *Daxx* or *Pml* in control mESCs had little effect on the level of TIFs (Figures 6I and S6E). In contrast, depleting *Daxx* and *Pml* individually or together led to significantly more TIFs in mutant mESCs (Figure 6I). When we examined pan-nuclear DNA damage, *Daxx* KD alone had little effect on either wild-type or mutant cells, while *Pml* KD led to modest but reproducible increases in pan-nuclear γ H2AX signals in mutant cells (Figure S6F). However, in mutant cells with combined *Daxx/Pml* KD, a significant increase in pan-nuclear γ H2AX staining was apparent (Figures 6J and S6G), suggesting

DAXX and PML may function synergistically with TIN2 to ensure telomere integrity and genome stability in mESCs. Collectively, our findings support the model where *Tin2*^{S341X} mESCs display drastically reduced *Tin2* expression, ALT-associated phenotypes, and elevated recruitment of DAXX/ATR proteins and PML bodies to telomeres (Figure 6K). In the mutant cells, telomeres become more unstable as DAXX/ATR proteins and PML bodies disassociate from telomeres upon differentiating, which leads to widespread chromatin instability and profound differentiation defects (Figure 6K).

DISCUSSION

The majority of work on telomere dysfunction has focused on cancer and somatic cells; the consequences in ESCs are much less studied and poorly understood. Recent evidence

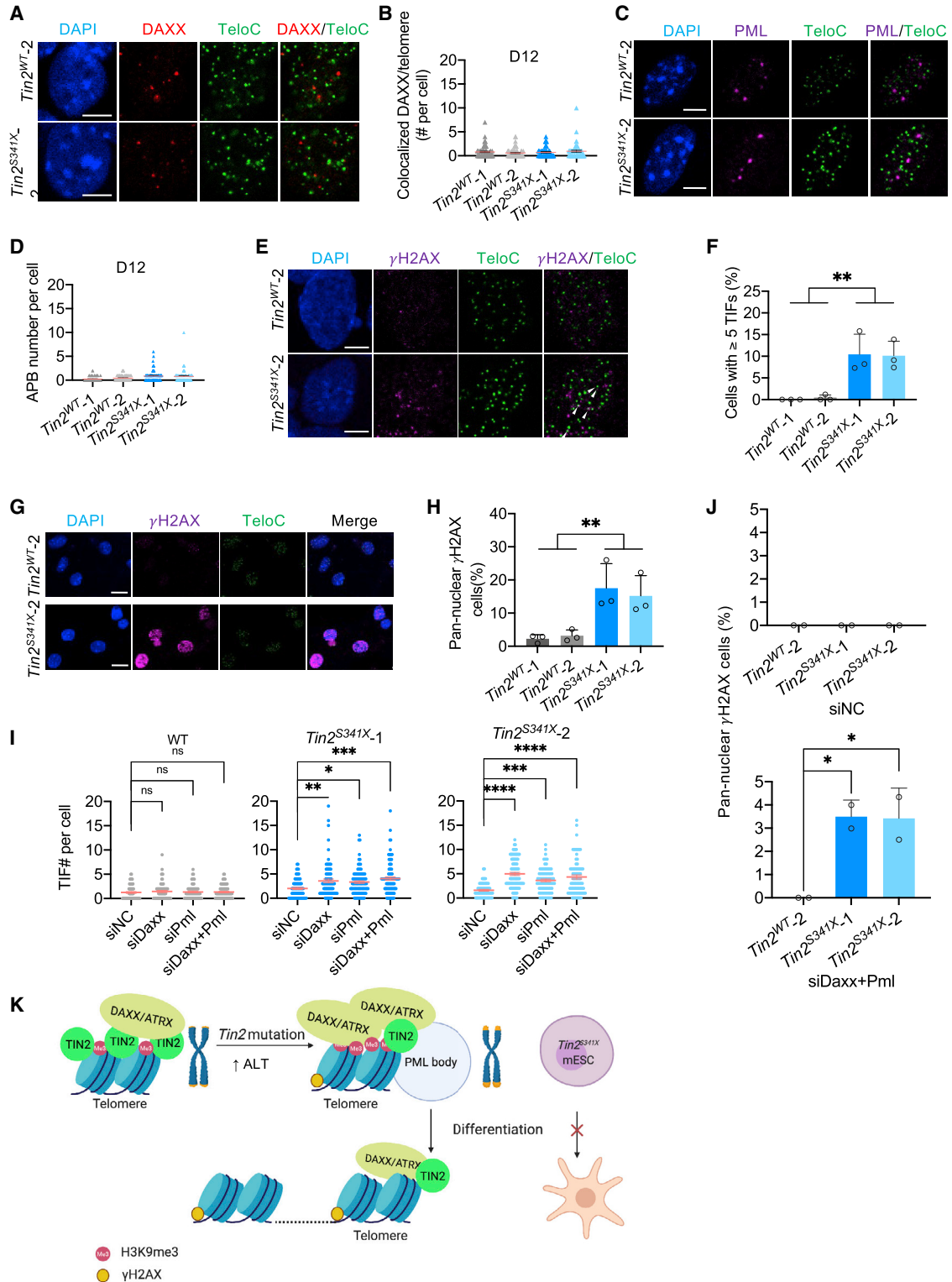


Figure 6. Mutant mESCs exhibit decreased telomere association of DAXX/ATR and PML upon differentiation

mESCs were differentiated to ectoderm lineage and analyzed at day 12 (D12).

(A–D) Cells were analyzed by IF-FISH using a telomere probe (green) together with an antibody against DAXX (red; A) or PML (purple; C). Representative images from each genotype are shown with scale bars of 5 μ m. Telomere-localized DAXX (B) and

(legend continued on next page)



from mESCs demonstrates that TRF2 is dispensable and suggests that mESCs may utilize a unique telomere protection mechanism in cases of dysfunctional telomere proteins (Markiewicz-Potoczny et al., 2020; Ruis et al., 2020). In this study, we showed that the *Tin2*^{S341X} caused TIN2 deficiency and the mutant mESCs display many of the characteristics associated with ALT cells, likely due to disrupted telomere maintenance pathways and the activation of ALT-mediating factors. Likewise, *Trf2*^{-/-} mESCs were reported to activate *Zscan4* and other 2C-related genes (Markiewicz-Potoczny et al., 2020). ALT-associated chromatin remodelers and PML bodies were found to be enriched at telomeres in *Trf1* KO MEFs (Porreca et al., 2020). Taken together, these data suggest loss of core telomere regulators during mouse early embryogenesis tends to promote ALT-associated phenotypes.

Telomere instability can prevent mESCs from normal differentiation, as evidenced by *Terc*^{-/-} mESCs that had short telomeres, reduced pluripotency potential, and difficulties in maintaining the differentiated state *in vitro* (Huang et al., 2011; Pucci et al., 2013). When we induced *Tin2*^{S341X} mESCs to differentiate into neural progenitor cells, they displayed widespread DNA damage, an observation in line with findings that newly generated neurons were hypersensitive to telomere dysfunction and DNA damage (Cheng et al., 2007).

The expression of subtelomeric genes appears more affected in *Tin2*^{S341X} mESCs, and several of them, such as *Isg15* and *Hoxc10*, are developmental process related. Gene ontology analysis on genome-wide subtelomeric genes also found several developmental processes to be enriched (data not shown). Whether and how telomere defects may affect developmental genes at subtelomeric regions warrants further investigation.

We hypothesize that telomeres may be differentially regulated in undifferentiated versus differentiated mESCs. In *Tin2*^{S341X} cells, chromatin remodeling factors, such as DAXX/ATRAX and PML bodies, were recruited to telomeres

in undifferentiated mESCs but dissociated from telomeres upon differentiation. How such dissociation occurs remains unclear. PML bodies are often enriched in gene-rich and transcriptionally active regions (Wang et al., 2004). DAXX/ATRAX mediate the deposition of the histone variant H3.3 to telomeres and other heterochromatin regions (Wong et al., 2009), while genome-wide profiling has indicated changes in H3.3-binding sites following mESC differentiation into neural progenitor cells (NPCs) (Goldberg et al., 2010). We thus speculate that perhaps DAXX/ATRAX and PML bodies can translocate to other regions of the chromatin in response to differentiation-induced gene expression and/or changes in chromatin structures.

Notably, there have been conflicting reports on telomeric histone modifications in ALT cells. For instance, while global H3K9me3 decrease is linked to ALT phenotypes (Episkopou et al., 2014), it has also been shown that typical ALT cells, such as U2OS, have relatively high levels of telomeric H3K9me3, but most non-ALT laboratory cell lines lack telomeric H3K9me3 marks under normal culture conditions (Cubiles et al., 2018). Increased telomeric H3K9me3 may even promote the appearance of ALT features in mESCs (Gauchier et al., 2019). Further studies in these fields will help uncover how dysfunction in telomere regulators affects telomere chromatin status in ESCs and how such changes impact the ESC differentiation process.

In patients, premature termination mutations are among major TIN2 pathogenic mutations. For example, *TINF2/TIN2 K280RfsX36* in DC patients resulted in earlier disease onset, more severe symptoms, and reduced expression of the truncated TIN2 protein (Sasa et al., 2012). Other premature terminations are also associated with elongated telomeres in several cancers (He et al., 2020; Schmutz et al., 2020). Premature termination mutations on TIN2L-specific exons have also been noted in clinical studies. For example, ClinVar

PML (D) were quantified and plotted. Lines are mean ± SEM. For each protein, >70 cells from two independent experiments were analyzed.

(E–H) Cells were analyzed by IF-FISH using an anti-γH2AX antibody (purple) and a telomere probe (green). Representative images from each genotype are shown in (E) with scale bars of 5 μm and in (G) with scale bars of 20 μm. Signals from >300 cells (three independent experiments) were quantified and plotted for telomeric (F) and pan-nuclear (H) γH2AX signals. Error bars indicate SD.

(I and J) Cells were transfected with siRNAs targeting *Daxx* and *Pml* either alone or together. At 48 h after transfection, IF-FISH using an anti-γH2AX antibody and a telomere probe was performed. TIFs were quantified and plotted in (I). Pan-γH2AX quantification in control and *Daxx/Pml* double KD cells are shown in (J). Greater than eighty cells from two independent experiments were analyzed. Error bars indicate SD.

(K) Based on our model, the *Tin2*^{S341X} mutation reduces *Tin2* expression and promotes ALT-associated phenotypes, such as long telomeres and increased telomeric association of PML bodies in undifferentiated mESCs, which is also accompanied by enrichment of DAXX/ATRAX and H3K9me3 on telomeres. DAXX/ATRAX and PML dissociate from telomeres following differentiation induction in these mutant cells, leading to DNA damage at telomeres and other genomic regions.

For (B, D, F, and H), t test was used to calculate significance. For (I and J), one-way ANOVA was used. *p < 0.05; **p < 0.01; ***p < 0.001; ****p < 0.0001; ns, p > 0.05.



VCV000575752 has recorded *TINF2/TIN2* c.1090dup p.Leu364Profs*9 found in a pediatric patient with motor delay and hypertonia (unpublished data). In our study, the *Tin2*^{S341X} mutation in exon7 reduced *Tin2* expression and re-introducing either TIN2 isoform yielded comparable results in *Tin2*^{S341X} mESCs. These findings suggest decreased *Tin2* expression is likely the main culprit for the phenotypes and support comparable functions for the two isoforms. How TIN2S and TIN2L may function differentially in other aspects warrants further exploration. More in-depth molecular and clinical research should shed light on how TIN2S and TIN2L may function differentially and contribute to human diseases.

EXPERIMENTAL PROCEDURES

CRISPR-Cas9-mediated knockin of a stop codon in the mouse *Tinf2/Tin2* locus

All experiments involving animals were performed in accordance with the guidelines approved by the Institutional Animal Care and Use Committee of Sun Yat-sen University, People's Republic of China. C57B₆/NJ mice were used in this study. Embryo injection and founder line construction was done by Shanghai Bangyao BioTech. Two heterozygous animals (out of 8) with the desired mutation were set up as founders and back-crossed for six generations. Genotyping was done by PCR and Sanger sequencing. Genotyping primers, CRISPR single-guide RNA (sgRNA), and donor template sequences are shown in Table S1.

IF staining and IF-FISH

Cells were plated on 0.2% gelatin-coated glass coverslips, fixed with 2% paraformaldehyde, and permeabilized in 0.5% Triton X-100 (in PBS) before further analysis. For IF-FISH, an additional incubation with PNA-(CCCTAA)₃-fluorescein isothiocyanate (FITC) probe (Panagene) was performed at 37°C for 2 h after secondary antibody incubation. Slides were preserved in Vectashield mounting media with DAPI. Fluorescence microscopy was performed on a Lightening STED SP8 (Leica) microscope. All antibodies used in this study are listed in Table S2. For IF-FISH, >120 cells from three independent experiments were analyzed unless otherwise noted. For TIN2 signal intensity analysis, the TFL-TELO program was used, and the intensities of the dots with TeloC signals but no TIN2 signals were counted as 0.

ChIP and slot blotting

We crosslinked 1×10^7 cells with 1% formaldehyde at room temperature for 5 min and then quenched in 125 mM glycine. Sonicated and pre-cleared lysates were then incubated with appropriate antibodies. The eluted DNA was purified by phenol:chloroform extraction, slot blotted onto Hybond-N+ membranes (GE Amersham), and probed with biotin-labeled probes. Signal intensity was measured by ImageJ. Telo probe was biotin-TTAGGGT TAGGGTTAGGGT. B1(Alu) probe was biotin-TAATCCCAGC ACTTGGG.

Statistical analysis

For *Tin2*^{WT-1}, *Tin2*^{WT-2}, *Tin2*^{S341X-1}, and *Tin2*^{S341X-2}, Student's t test with 95% confidence level was used to compare means of wild type and mutant. For multiple samples, one-way ANOVA followed by Dunnett's multiple comparison test with 95% confidence level was performed. For multiple samples across multiple time points, two-way ANOVA was performed. A $p < 0.05$ was considered statistically significant.

Data and code availability

RNA-seq data from this study can be found in GEO: GSE156514.

SUPPLEMENTAL INFORMATION

Supplemental information can be found online at <https://doi.org/10.1016/j.stemcr.2022.03.005>.

AUTHOR CONTRIBUTIONS

Z.S., Y.H., and S.Y. conceived the project. S.Y. conducted most of the experiments and data analysis. Y.H. designed the truncation mutation. F.Z. performed the experiments about embryos and constructed mESC lines. W.C. performed Q-TRAP and methylation assay and assisted with other experiments. C.W. performed C-circle experiment. Z.H. performed the TRF assay. S.L. assisted with embryo experiments and other assays. S.Y. and K.W. analyzed the RNA-seq data. S.Y. wrote the manuscript. Z.S., D.L., and Y.H. revised the manuscript. S.Y., Z.S., Y.H., Y.C., W.C., S.L., W.M., J.H., and D.L. discussed the project.

CONFLICTS OF INTERESTS

The authors declare no competing interests.

ACKNOWLEDGMENTS

This work was supported by the National Key Research and Development Program of China (2017YFA0102801), the National Natural Science Foundation of China (81871109, 82071587, 31930058, 91640119, and 81330055), Guangdong Basic and Applied Basic Research Foundation (2020A1515010462), and the Zhujiang Program of Science and Technology Nova in Guangzhou (grant 201710010042). We thank all members of the Songyang lab for their advice and support. We are grateful to Dr. Titia de Lange (Rockefeller University, US) for her kind gift of the anti-TIN2 antibody, Invitae Corporation for the information of CinVar VCV000575752 carrier, and Minyue Qi for advice and assistance in RNA-seq analysis (University of Hamburg, Germany).

Received: August 25, 2021

Revised: March 7, 2022

Accepted: March 8, 2022

Published: April 7, 2022

REFERENCES

Bryan, T.M., Englezou, A., Gupta, J., Bacchetti, S., and Reddel, R.R. (1995). Telomere elongation in immortal human cells without detectable telomerase activity. *EMBO J.* 14, 4240–4248.



- Celli, G.B., and de Lange, T. (2005). DNA processing is not required for ATM-mediated telomere damage response after TRF2 deletion. *Nat. Cell Biol.* *7*, 712–718. <https://doi.org/10.1038/ncb1275>.
- Cesare, A.J., and Griffith, J.D. (2004). Telomeric DNA in ALT cells is characterized by free telomeric circles and heterogeneous t-loops. *Mol. Cell Biol.* *24*, 9948. <https://doi.org/10.1128/MCB.24.22.9948-9957.2004>.
- Chen, L.-Y., Zhang, Y., Zhang, Q., Li, H., Luo, Z., Fang, H., Kim, S.H., Qin, L., Yotnda, P., Xu, J., et al. (2012). Mitochondrial localization of telomeric protein TIN2 links telomere regulation to metabolic control. *Mol. Cell* *47*, 839–850. <https://doi.org/10.1016/j.molcel.2012.07.002>.
- Cheng, A., Shin-ya, K., Wan, R., Tang, S.-c., Miura, T., Tang, H., Khatri, R., Gleichman, M., Ouyang, X., Liu, D., et al. (2007). Telomere protection mechanisms change during neurogenesis and neuronal maturation: newly generated neurons are hypersensitive to telomere and DNA damage. *J. Neurosci.* *27*, 3722–3733. <https://doi.org/10.1523/JNEUROSCI.0590-07.2007>.
- Chiang, Y.J., Kim, S.-H., Tessarollo, L., Campisi, J., and Hodes, R.J. (2004). Telomere-associated protein TIN2 is essential for early embryonic development through a telomerase-independent pathway. *Mol. Cell Biol.* *24*, 6631–6634. <https://doi.org/10.1128/MCB.24.15.6631-6634.2004>.
- Cubiles, M.D., Barroso, S., Vaquero-Sedas, M.I., Enguix, A., Aguilera, A., and Vega-Palas, M.A. (2018). Epigenetic features of human telomeres. *Nucleic Acids Res.* *46*, 2347–2355. <https://doi.org/10.1093/nar/gky006>.
- de Feraudy, S., Revet, I., Bezrookove, V., Feeney, L., and Cleaver, J.E. (2010). A minority of foci or pan-nuclear apoptotic staining of γ H2AX in the S phase after UV damage contain DNA double-strand breaks. *Proc. Natl. Acad. Sci. U S A* *107*, 6870. <https://doi.org/10.1073/pnas.1002175107>.
- de Lange, T. (2005). Shelterin: the protein complex that shapes and safeguards human telomeres. *Genes Dev.* *19*, 2100–2110. <https://doi.org/10.1101/gad.1346005>.
- Dellaire, G., Ching, R.W., Ahmed, K., Jalali, F., Tse, K.C.K., Bristow, R.G., and Bazett-Jones, D.P. (2006). Promyelocytic leukemia nuclear bodies behave as DNA damage sensors whose response to DNA double-strand breaks is regulated by NBS1 and the kinases ATM, Chk2, and ATR. *J. Cell Biol.* *175*, 55–66. <https://doi.org/10.1083/jcb.200604009>.
- Episkopou, H., Draskovic, I., Van Beneden, A., Tilman, G., Mattiussi, M., Gobin, M., Arnoult, N., Londoño-Vallejo, A., and Decottignies, A. (2014). Alternative Lengthening of Telomeres is characterized by reduced compaction of telomeric chromatin. *Nucleic Acids Res.* *42*, 4391–4405. <https://doi.org/10.1093/nar/gku114>.
- Falco, G., Lee, S.-L., Stanghellini, I., Bassey, U.C., Hamatani, T., and Ko, M.S.H. (2007). Zscan4: a novel gene expressed exclusively in late 2-cell embryos and embryonic stem cells. *Dev. Biol.* *307*, 539–550. <https://doi.org/10.1016/j.ydbio.2007.05.003>.
- Frank, A.K., Tran, D.C., Qu, R.W., Stohr, B.A., Segal, D.J., and Xu, L. (2015). The shelterin TIN2 subunit mediates recruitment of telomerase to telomeres. *PLoS Genet.* *11*, e1005410. <https://doi.org/10.1371/journal.pgen.1005410>.
- Gauchier, M., Kan, S., Barral, A., Sauzet, S., Agirre, E., Bonnell, E., Saksouk, N., Barth, T.K., Ide, S., Urbach, S., et al. (2019). SETDB1-dependent heterochromatin stimulates alternative lengthening of telomeres. *Sci. Adv.* *5*, eaav3673. <https://doi.org/10.1126/sciadv.aav3673>.
- Goldberg, A.D., Banaszynski, L.A., Noh, K.M., Lewis, P.W., Elsaesser, S.J., Stadler, S., Dewell, S., Law, M., Guo, X., Li, X., et al. (2010). Distinct factors control histone variant H3.3 localization at specific genomic regions. *Cell* *140*, 678–691. <https://doi.org/10.1016/j.cell.2010.01.003>.
- Gonzalo, S., Jaco, I., Fraga, M.F., Chen, T., Li, E., Esteller, M., and Blasco, M.A. (2006). DNA methyltransferases control telomere length and telomere recombination in mammalian cells. *Nat. Cell Biol.* *8*, 416–424. <https://doi.org/10.1038/ncb1386>.
- He, H., Li, W., Comiskey, D.F., Liyanarachchi, S., Nieminen, T.T., Wang, Y., DeLap, K.E., Brock, P., and de la Chapelle, A. (2020). A truncating germline mutation of TIN2 in individuals with thyroid cancer or melanoma results in longer telomeres. *Thyroid* *30*, 204–213. <https://doi.org/10.1089/thy.2019.0156>.
- He, Q., Kim, H., Huang, R., Lu, W., Tang, M., Shi, F., Yang, D., Zhang, X., Huang, J., Liu, D., and Songyang, Z. (2015). The Daxx/Atrx complex protects tandem repetitive elements during DNA hypomethylation by promoting H3K9 trimethylation. *Cell Stem Cell* *17*, 273–286. <https://doi.org/10.1016/j.stem.2015.07.022>.
- Henson, J.D., Cao, Y., Huschtscha, L.I., Chang, A.C., Au, A.Y.M., Pickett, H.A., and Reddel, R.R. (2009). DNA C-circles are specific and quantifiable markers of alternative-lengthening-of-telomeres activity. *Nat. Biotech.* *27*, 1181–1185. <https://doi.org/10.1038/nbt.1587>.
- Hitoshi, S., Seaberg, R.M., Kosciak, C., Alexson, T., Kusunoki, S., Kanazawa, I., Tsuji, S., and van der Kooy, D. (2004). Primitive neural stem cells from the mammalian epiblast differentiate to definitive neural stem cells under the control of Notch signaling. *Genes Dev.* *18*, 1806–1811. <https://doi.org/10.1101/gad.1208404>.
- Hockemeyer, D., Daniels, J.P., Takai, H., and de Lange, T. (2006). Recent expansion of the telomeric complex in rodents: two distinct POT1 proteins protect mouse telomeres. *Cell* *126*, 63–77. <https://doi.org/10.1016/j.cell.2006.04.044>.
- Huang, J., Wang, F., Okuka, M., Liu, N., Ji, G., Ye, X., Zuo, B., Li, M., Liang, P., Ge, W.W., et al. (2011). Association of telomere length with authentic pluripotency of ES/iPS cells. *Cell Res.* *21*, 779–792. <https://doi.org/10.1038/cr.2011.16>.
- Hung, S.S., Wong, R.C., Sharov, A.A., Nakatake, Y., Yu, H., and Ko, M.S. (2013). Repression of global protein synthesis by Eif1a-like genes that are expressed specifically in the two-cell embryos and the transient Zscan4-positive state of embryonic stem cells. *DNA Res.* *20*, 391–402. <https://doi.org/10.1093/dnares/dst018>.
- Juhasz, S., Elbakry, A., Mathes, A., and Lohrich, M. (2018). ATRX promotes DNA repair synthesis and sister chromatid exchange during homologous recombination. *Mol. Cell* *71*, 11–24.e7. <https://doi.org/10.1016/j.molcel.2018.05.014>.



- Kaminker, P.G., Kim, S.-H., Desprez, P.-Y., and Campisi, J. (2009). A novel form of the telomere-associated protein TIN2 localizes to the nuclear matrix. *Cell Cycle* 8, 931–939. <https://doi.org/10.4161/cc.8.6.7941>.
- Karlseder, J., Kachatrian, L., Takai, H., Mercer, K., Hingorani, S., Jacks, T., and de Lange, T. (2003). Targeted deletion reveals an essential function for the telomere length regulator Trf1. *Mol. Cell Biol.* 23, 6533–6541. <https://doi.org/10.1128/MCB.23.18.6533-6541.2003>.
- Kibe, T., Osawa, G.A., Keegan, C.E., and de Lange, T. (2010). Telomere protection by TPP1 is mediated by POT1a and POT1b. *Mol. Cell Biol.* 30, 1059. <https://doi.org/10.1128/MCB.01498-09>.
- Kim, H., Li, F., He, Q., Deng, T., Xu, J., Jin, F., Coarfa, C., Putluri, N., Liu, D., and Songyang, Z. (2017). Systematic analysis of human telomeric dysfunction using inducible telosome/shelterin CRISPR/Cas9 knockout cells. *Cell Discov.* 3, 17034. <https://doi.org/10.1038/celldisc.2017.34>.
- Kim, S.-h., Beausejour, C., Davalos, A.R., Kaminker, P., Heo, S.-J., and Campisi, J. (2004). TIN2 mediates functions of TRF2 at human telomeres. *J. Bio Chem.* 279, 43799–43804. <https://doi.org/10.1074/jbc.M408652000>.
- Kim, S.-h., Davalos, A.R., Heo, S.-J., Rodier, F., Zou, Y., Beausejour, C., Kaminker, P., Yannoni, S.M., and Campisi, J. (2008). Telomere dysfunction and cell survival: roles for distinct TIN2-containing complexes. *J. Cell Biol.* 181, 447. <https://doi.org/10.1083/JCB.200710028>.
- Kim, S.H., Kaminker, P., and Campisi, J. (1999). TIN2, a new regulator of telomere length in human cells. *Nat. Genet.* 23, 405–412. <https://doi.org/10.1038/70508>.
- Lewis, P.W., Elsaesser, S.J., Noh, K.-M., Stadler, S.C., and Allis, C.D. (2010). Daxx is an H3.3-specific histone chaperone and cooperates with ATRX in replication-independent chromatin assembly at telomeres. *Proc. Natl. Acad. Sci. U S A* 107, 14075. <https://doi.org/10.1073/pnas.1008850107>.
- Liu, D., O'Connor, M.S., Qin, J., and Songyang, Z. (2004). Telosome, a mammalian telomere-associated complex formed by multiple telomeric proteins. *J. Biol. Chem.* 279, 51338–51342. <https://doi.org/10.1074/jbc.M409293200>.
- Londono-Vallejo, J.A., Der-Sarkissian, H., Cazes, L., Bacchetti, S., and Reddel, R.R. (2004). Alternative lengthening of telomeres is characterized by high rates of telomeric exchange. *Cancer Res.* 64, 2324–2327.
- Lykke-Andersen, S., and Jensen, T.H. (2015). Nonsense-mediated mRNA decay: an intricate machinery that shapes transcriptomes. *Nat. Rev. Mol. Cell Biol.* 16, 665–677. <https://doi.org/10.1038/nrm4063>.
- Macfarlan, T.S., Gifford, W.D., Driscoll, S., Lettieri, K., Rowe, H.M., Bonanomi, D., Firth, A., Singer, O., Trono, D., and Pfaff, S.L. (2012). Embryonic stem cell potency fluctuates with endogenous retrovirus activity. *Nature* 487, 57–63. <https://doi.org/10.1038/nature11244>.
- Marchesini, M., Matocci, R., Tasselli, L., Cambiaghi, V., Orleth, A., Furia, L., Marinelli, C., Lombardi, S., Sammarelli, G., Aversa, F., et al. (2016). PML is required for telomere stability in non-neoplastic human cells. *Oncogene* 35, 1811–1821. <https://doi.org/10.1038/onc.2015.246>.
- Markiewicz-Potoczny, M., Lobanova, A., Loeb, A.M., Kirak, O., Olbrich, T., Ruiz, S., and Lazznerini Denchi, E. (2020). TRF2-mediated telomere protection is dispensable in pluripotent stem cells. *Nature* <https://doi.org/10.1038/s41586-020-2959-4>.
- Martinez, P., and Blasco, M.A. (2017). Telomere-driven diseases and telomere-targeting therapies. *J. Cell Biol.* 216, 875–887. <https://doi.org/10.1083/jcb.201610111>.
- Moeglin, E., Desplancq, D., Conic, S., Oulad-Abdelghani, M., Stoessel, A., Chiper, M., Vigneron, M., Didier, P., Tora, L., and Weiss, E. (2019). Uniform widespread nuclear phosphorylation of histone H2AX is an indicator of lethal DNA replication stress. *Cancers* 11. <https://doi.org/10.3390/cancers11030355>.
- Nelson, N.D., Dodson, L.M., Escudero, L., Sukumar, A.T., Williams, C.L., Mihalek, I., Baldan, A., Baird, D.M., and Bertuch, A.A. (2018). The C-terminal extension unique to the long isoform of the shelterin component TIN2 enhances its interaction with TRF2 in a phosphorylation- and dyskeratosis congenita cluster-dependent fashion. *Mol. Cell Biol.* 38. <https://doi.org/10.1128/MCB.00025-18>.
- Niida, H., Shinkai, Y., Hande, M.P., Matsumoto, T., Takehara, S., Tachibana, M., Oshimura, M., Lansdorp, P.M., and Furuichi, Y. (2000). Telomere maintenance in telomerase-deficient mouse embryonic stem cells: characterization of an amplified telomeric DNA. *Mol. Cell Biol.* 20, 4115–4127. <https://doi.org/10.1128/mcb.20.11.4115-4127.2000>.
- Plantinga, M.J., Pascarelli, K.M., Merkel, A.S., Lazar, A.J., von Mehren, M., Lev, D., and Broccoli, D. (2013). Telomerase suppresses formation of ALT-associated single-stranded telomeric C-circles. *Mol. Cancer Res.* 11, 557–567. <https://doi.org/10.1158/1541-7786.MCR-13-0013>.
- Porreca, R.M., Herrera-Moyano, E., Skourti, E., Law, P.P., Gonzalez Franco, R., Montoya, A., Faull, P., Kramer, H., and Vannier, J.-B. (2020). TRF1 averts chromatin remodelling, recombination and replication dependent-break induced replication at mouse telomeres. *Elife* 9, e49817. <https://doi.org/10.7554/eLife.49817>.
- Pucci, F., Gardano, L., and Harrington, L. (2013). Short telomeres in ESCs lead to unstable differentiation. *Stem Cell* 12, 479–486. <https://doi.org/10.1016/j.stem.2013.01.018>.
- Ruis, P., Van Ly, D., Borel, V., Kafer, G.R., McCarthy, A., Howell, S., Blassberg, R., Snijders, A.P., Briscoe, J., Niakan, K.K., et al. (2020). TRF2-independent chromosome end protection during pluripotency. *Nature* <https://doi.org/10.1038/s41586-020-2960-y>.
- Sasa, G.S., Ribes-Zamora, A., Nelson, N.D., and Bertuch, A.A. (2012). Three novel truncating TIN2 mutations causing severe dyskeratosis congenita in early childhood. *Clin. Genet.* 81, 470–478. <https://doi.org/10.1111/j.1399-0004.2011.01658.x>.
- Savage, S.A., Giri, N., Baerlocher, G.M., Orr, N., Lansdorp, P.M., and Alter, B.P. (2008). TIN2, a component of the shelterin telomere protection complex, is mutated in dyskeratosis congenita. *Am. J. Hum. Genet.* 82, 501–509. <https://doi.org/10.1016/j.ajhg.2007.10.004>.
- Schmutz, I., Mensenkamp, A.R., Takai, K.K., Haadsma, M., Spruijt, L., de Voer, R.M., Choo, S.S., Lorbeer, F.K., van Grinsven, E.J., Hockemeyer, D., et al. (2020). TIN2 is a haploinsufficient tumor



suppressor that limits telomere length. *Elife* 9. <https://doi.org/10.7554/eLife.61235>.

Shay, J.W., and Wright, W.E. (2019). Telomeres and telomerase: three decades of progress. *Nat. Rev. Genet.* 20, 299–309. <https://doi.org/10.1038/s41576-019-0099-1>.

Storm, M.P., Kumpfmüller, B., Bone, H.K., Buchholz, M., Sanchez Ripoll, Y., Chaudhuri, J.B., Niwa, H., Tosh, D., and Welham, M.J. (2014). Zscan4 is regulated by PI3-kinase and DNA-damaging agents and directly interacts with the transcriptional repressors LSD1 and CtBP2 in mouse embryonic stem cells. *PLoS One* 9, e89821. <https://doi.org/10.1371/journal.pone.0089821>.

Takai, H., Smogorzewska, A., and de Lange, T. (2003). DNA damage foci at dysfunctional telomeres. *Curr. Biol.* 13, 1549–1556. [https://doi.org/10.1016/s0960-9822\(03\)00542-6](https://doi.org/10.1016/s0960-9822(03)00542-6).

Walne, A.J., Vulliamy, T., Beswick, R., Kirwan, M., and Dokal, I. (2008). TIN2 mutations result in very short telomeres: analysis of a large cohort of patients with dyskeratosis congenita and related bone marrow failure syndromes. *Blood* 112, 3594–3600. <https://doi.org/10.1182/blood-2008-05-153445>.

Wang, J., Shiels, C., Sasieni, P., Wu, P.J., Islam, S.A., Freemont, P.S., and Sheer, D. (2004). Promyelocytic leukemia nuclear bodies associate with transcriptionally active genomic regions. *J. Cell Biol.* 164, 515–526. <https://doi.org/10.1083/jcb.200305142>.

Wong, L.H., Ren, H., Williams, E., McGhie, J., Ahn, S., Sim, M., Tam, A., Earle, E., Anderson, M.A., Mann, J., and Choo, K.H. (2009). Histone H3.3 incorporation provides a unique and functionally essential telomeric chromatin in embryonic stem cells. *Genome Res.* 19, 404–414. <https://doi.org/10.1101/gr.084947.108>.

Ye, J.Z.-S., and de Lange, T. (2004). TIN2 is a tankyrase 1 PARP modulator in the TRF1 telomere length control complex. *Nat. Genet.* 36, 618–623. <https://doi.org/10.1038/ng1360>.

Yeager, T.R., Neumann, A.A., Englezou, A., Huschtscha, L.I., Noble, J.R., and Reddel, R.R. (1999). Telomerase-negative immortalized human cells contain a novel type of promyelocytic leukemia (PML) body. *Cancer Res.* 59, 4175–4179.

Zalzman, M., Falco, G., Sharova, L.V., Nishiyama, A., Thomas, M., Lee, S.L., Stagg, C.A., Hoang, H.G., Yang, H.T., Indig, F.E., et al. (2010). Zscan4 regulates telomere elongation and genomic stability in ES cells. *Nature* 464, 858–863. <https://doi.org/10.1038/nature08882>.

Zhang, W., Chen, F., Chen, R., Xie, D., Yang, J., Zhao, X., Guo, R., Zhang, Y., Shen, Y., Goke, J., et al. (2019). Zscan4c activates endogenous retrovirus MERVL and cleavage embryo genes. *Nucleic Acids Res.* 47, 8485–8501. <https://doi.org/10.1093/nar/gkz594>.